Chinese Physics Letters

LETTER

Fast and Coherent Transfer of Atomic Qubits in Optical Tweezers Using Fiber Array Architecture

Cite as: Jia-Chao Wang *et al*. 2026 *Chin. Phys. Lett.* **43** 060601

DOI CSTR

Recommended Articles

Direct Generation of an Array with 78400 Optical Tweezers Using a Single Metasurface
Yuqing Wang *et al*.
Chin. Phys. Lett. **43**, 010606 (2026)

Coherent Optical Frequency Transfer via a 490 km Noisy Fiber Link
Xiang Zhang *et al*.
Chin. Phys. Lett. **39**, 044201 (2022)

Managing Quantum Heat Transfer in a Nonequilibrium Qubit-Phonon Hybrid System with Coherent Phonon States
Chen Wang, Lu-Qin Wang, and Jie Ren
Chin. Phys. Lett. **38**, 010501 (2021)

Efficient Two-Dimensional Defect-Free Dual-Species Atom Arrays Rearrangement Algorithm with Near-Fewest Atom Moves
Zhi-Jin Tao, Li-Geng Yu, Peng Xu, Jia-Yi Hou, Xiao-Dong He, and Ming-Sheng Zhan
Chin. Phys. Lett. **39**, 083701 (2022)

Robust Transfer of Optical Frequency over 500km Fiber Link with Instability of 10^{-21}
Qian Zhou, Xiang Zhang, Qi Zang, Mengfan Wu, Dan Wang, Jie Liu, Ruifang Dong, Tao Liu, and Shougang Zhang
Chin. Phys. Lett. **41**, (2024)

Enhancing the Coherence Time of a Neutral Atom by an Optical Quartic Trap
Haobo Chang, Zhuangzhuang Tian, Xin Lv, Mengna Yang, Zhihui Wang, Qi Guo, Pengfei Yang, Pengfei Zhang, Gang Li, and Tiancai Zhang
Chin. Phys. Lett. **42**, 110303 (2025)

A series journal of Chinese Physical Society distributed by IOP Publishing

iopscience.iop.org/cpl | cpl.iphy.ac.cn

Chinese Physics Letters

Chin. Phys. Lett. **43** 060601 (2026)

LETTER

DOI: 10.1088/0256-307X/43/6/060601
CSTR: 32039.14.0256-307X.43.6.060601

Fast and Coherent Transfer of Atomic Qubits in Optical Tweezers Using Fiber Array Architecture

Jia-Chao Wang(王家超)[1,2], Zai-Zheng Zhang(张再正)[1,2], Xiao Li(李潇)[1,*], Guang-Wei Wang(王光伟)[1,2], Xiao-Dong He(何晓东)[1], Min Liu(刘敏)[1], and Peng Xu(许鹏)[1,3,*]

[1]Division of Precision Measurement Physics, Wuhan Institute of Physics and Mathematics, Innovation Academy for Precision Measurement Science and Technology, Chinese Academy of Sciences, Wuhan 430071, China
[2]School of Physical Sciences, University of Chinese Academy of Sciences, Beijing 100190, China
[3]Wuhan Institute of Quantum Technology, Wuhan 430206, China

[*]Corresponding authors. Email: lixiao@apm.ac.cn; xupeng@apm.ac.cn

Programmable neutral-atom arrays offer a promising route toward scalable quantum computing, where coherent qubit transfer enables non-local connectivity and reduces resource overhead. However, transfer speed and motional heating remain key bottlenecks for fast and deep quantum circuits. Here, we employ a fiber array neutral-atom quantum computing architecture with site-resolved control of trap depths to realize smooth amplitude exchange between static and moving traps, thereby enabling fast and coherent qubit transfer with ultralow motional heating. With a 10-μs *in situ* transfer between static and moving traps, we obtain a per-cycle heating rate of 0.156(9) μK, sustain over 500 cycles with negligible atom loss, and achieve a quantum state fidelity of 0.99992(5) per cycle. For inter-site transfer between two separated static traps, the operation takes 120 μs with 0.783(17) μK heating per transfer, and exhibits negligible atom loss for up to 100 repeated cycles with a fidelity of 0.9998(1) per transfer. Furthermore, through experimental studies of parallel transfer, we establish a model that elucidates the relationship between array inhomogeneity and the transfer heating rate. This fast, low-heating coherent transfer capability provides a practical route for improving both speed and fidelity in atom-shuttling based quantum computing.

Introduction

Neutral-atom arrays trapped in optical tweezers have emerged as a promising platform for quantum computation and quantum simulation [1−6]. A distinctive advantage of these systems is their ability to provide on-demand, non-local connectivity between qubits, which is particularly beneficial for logical-qubit encoding and logical gate operations [7−14]. Typically, realizing such non-local connectivity requires coherently transferring qubits between tweezer sites across the array, thereby bringing selected qubits into a desired configuration for interaction or addressing [9,15−20]. To date, this capability has been demonstrated using several approaches, including operating under magic-intensity trapping conditions to suppress differential light shifts [19], employing adiabatic protocols to minimize motional heating [9], and leveraging AI-assisted optimization of tweezer depths and positions to improve transfer fidelity and robustness [20].

However, current schemes lack independent, site-resolved control of the depth of each static trap (S-trap), which prevents smoothly ramping an individual S-trap depth to zero. Under this constraint, during extraction with a moving trap (M-trap), the atom experiences a residual potential from the S-trap, introducing an additional time-dependent perturbation. To suppress the resulting motional heating, *in situ* transfer is typically carried out on a relatively long timescale, often requiring hundreds of microseconds. Moreover, owing to accumulated heating, repeated transfers over just tens of cycles lead to noticeable atom loss [3], which constrains performance in high-speed, large-depth quantum circuits.

In this work, we leverage a fiber-array architecture with site-resolved, independent control of static-trap depths [5] to realize a fast coherent transfer scheme based on smooth amplitude exchange between static and moving traps [21]. Using this approach, we demonstrate *in situ* coherent transfer in 10 μs between static and moving traps with a per-cycle heating rate of 0.156(9) μK, sustaining 500 lossless cycles. Building on this *in situ* transfer and combining it with atom transport, we further demonstrate low-heating inter-site transfer between two separated static traps. Finally, we perform parallel inter-site transfer and establish a model that quantifies the dependence of the transfer heating rate on array inhomogeneity, informing the optimization of coherent transfer in large-scale arrays.

Experimental Setup

The experimental setup of the fiber-array-based atomic quantum computer has been described in detail in our previous work [5]. Each fiber serves as the interface for trapping and addressing an individual ^{87}Rb atom, simultaneously enabling scalability and independent control. In this work, we utilize fiber-array-based optical traps as S-traps, selecting six of them, each with independently controllable depth, and introduce an M-trap for qubit transport within the array (see Fig. 1). After emerging from the AOD, the M-trap beam first passes through a reflective 4f relay system with a 1 : 1 magnification, and is then combined with the S-trap beam using a beam splitter ($T : R = 9 : 1$).

For fast, low-heating *in situ* coherent transfer, precise alignment between the S-trap and M-trap is required. Radial alignment is achieved by scanning the AOD frequency and fitting the atom survival probability after repeated transfer cycles, while axial alignment is optimized by translating a mirror in the reflective 4f relay system. The measured trap-frequency difference between the M-trap and S-trap is below 3%. More details of the experimental setup are provided in the Supplementary Material.

Fast Coherent *in situ* Transfer of a Single Atomic Qubit

After aligning the S-trap and M-trap, we perform rapid trap-depth modulation to realize *in situ* qubit transfer. Ideally, perfect spatial overlap between the two traps maintains a constant effective trap depth during amplitude swapping, yielding zero heating regardless of

Received 11 March 2026; accepted 24 April 2026; published 1 June 2026
© 2026 Chinese Physical Society and IOP Publishing Ltd. All rights, including for text and data mining, AI training, and similar technologies, are reserved.

Check for updates

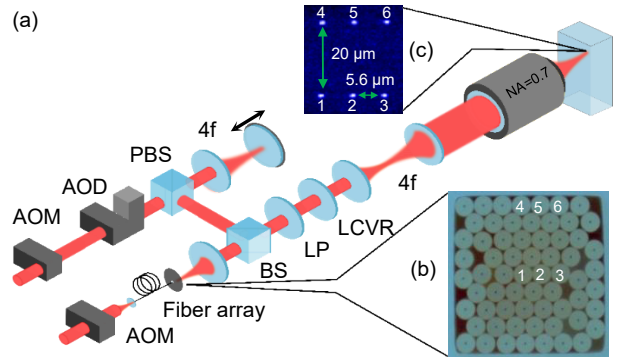

Fig. 1. Schematic of the experimental setup for coherent transfer. (a) The M-trap laser beam first passes through the acousto-optic modulator (AOM) and acousto-optic deflector (AOD). Then it is combined with the S-trap laser beam using a beam splitter (BS). The combined beams subsequently pass through a linear polarizer (LP) and a liquid crystal variable retarder (LCVR), followed by a 4f beam-expanding system and an objective, before finally entering the vacuum chamber. (b) The cross-section of the fiber array. Six traps are selected from the array for our experiment. (c) Fluorescence image of six single atoms trapped in selected traps.

the modulation waveform. In practice, however, thermal fluctuations and mechanical drifts introduce a slight spatial misalignment. In the small-misalignment limit, the amplitude exchange shifts the combined trap minimum, resulting in an effective short-distance transport of the atom that induces heating. To minimize this heating, we design the depth variation so that the effective spatial motion of the trap minimum follows a shortcuts-to-adiabaticity (STA) [22–25] trajectory, as detailed in the Supplementary Material. The depth variation of the M-trap is described by the following STA function:

$$x(t) = -20t^7 + 70t^6 - 84t^5 + 35t^4 \ (t, x \in [0,1]). \tag{1}$$

The normalized S-trap depth follows the function $1 - x(t)$ [as shown in the inset of Fig. 2(a)]. We maintain the effective trap depth U_0 of the combined S-trap and M-trap at 1 mK, with an amplitude swap time of 10 μs and a subsequent 20 μs wait time to confirm completion of the one-way transfer process. During this wait time, the initial trap remains off so that any untransferred atoms are lost, ensuring the measured survival strictly reflects a genuine transfer rather than the mere survival of the depth modulation. The atom survival probability decreases from 0.98 to around 0.9 after 1000 transfer cycles. The loss is mainly due to transfer induced atom heating [see Fig. 2(a)].

To analyze the heating rate, we adopt a theoretical description in which atoms in a dipole trap follow a Boltzmann distribution [26]. Here, we introduce a normalized temperature coefficient

$$\zeta = (T_0 + \Delta T \cdot n)/U_0, \tag{2}$$

where T_0 is the initial temperature, and ΔT is the heating per transfer, n is the number of transfer cycles. By integrating the Boltzmann energy distribution up to the trap depth, the survival probability of the atom remaining in the dipole trap after the truncation at the finite trap depth is given by

$$P(n) = P_0\left(1 - (1 + 1/\zeta + 1/(2\cdot\zeta^2))\cdot\exp(-1/\zeta)\right), \tag{3}$$

where P_0 is the initial atom survival probability. In our system, the initial atom temperature is 15 μK, corresponding to a 2D radial motional ground-state fraction of ~13.0% . We fitted the experimental data and obtained the per transfer cycle heating rates of Trap 2 and Trap 3 as 0.165(6) μK and 0.148(11) μK, respectively, which induce a reduction of ~0.2% in the radial motional ground-state fraction after the first transfer cycle.

Additionally, we employed quantum state tomography [27–29] to characterize the internal state fidelity of the atomic qubits during the transfer process. The two hyperfine levels of the ^{87}Rb clock transition are chosen as the basis states $|0\rangle = |F = 1, m_F = 0\rangle$ and $|1\rangle = |F = 2,$

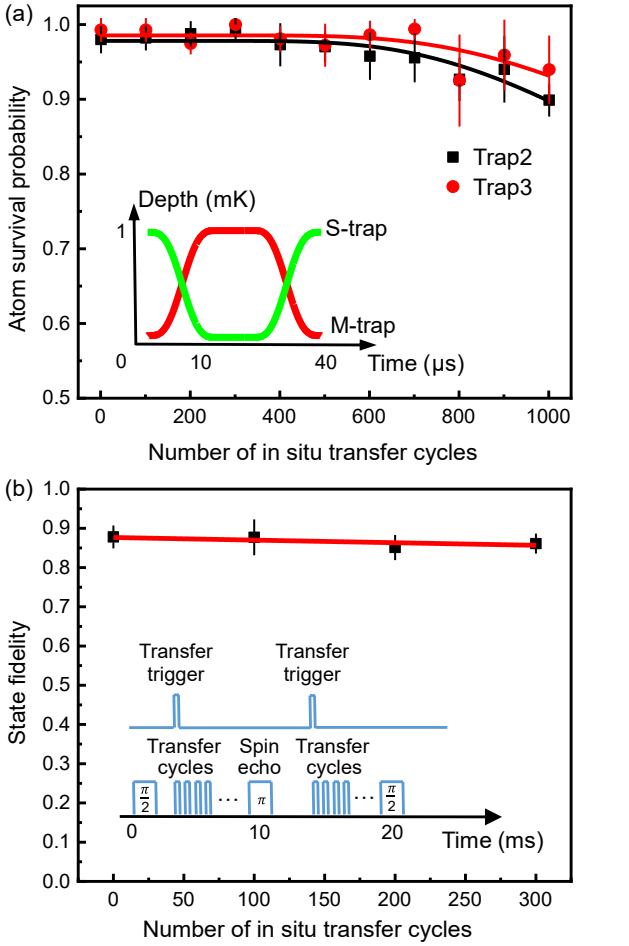

Fig. 2. Fast coherent *in situ* transfer of a single atomic qubit. (a) Atom survival probability after different numbers of transfer cycles between the M-trap and S-trap. Inset: the STA-modulated amplitude waveforms for the M-trap (green) and S-trap (red). (b) Internal-state fidelity after different numbers of transfer cycles fitted with an exponential decay function. Inset, the pulse sequence of quantum state tomography.

$m_F = 0\rangle$. By employing magic-intensity trapping and spin echo techniques, we have extended the coherence time of the atoms to over 100 ms, which is significantly longer than the coherent transfer time [19, 30]. We begin by preparing the atom in the $|0\rangle$ state with a raw fidelity above 0.95, followed by a resonant $\pi/2$ microwave pulse to prepare it in a superposition state. To suppress inhomogeneous dephasing, a spin-echo π pulse is inserted after 10 ms. Following an interval of 10 ms, a second $\pi/2$ pulse is applied. Coherent transfers are performed symmetrically about the π pulse, distributed across both intervals [see inset of Fig. 2(b)]. After completing this 20 ms sequence, the raw state fidelity is measured at 0.88(3), which has decreased by ~0.07 compared to the initial $|0\rangle$ state preparation. This is primarily due to the photon scattering induced fidelity loss in the 830 nm dipole trap with a depth of 1 mK. After 300 transfer cycles, the state fidelity remained at 0.86(3). The single transfer cycle fidelity obtained from exponential decay fitting is 0.99992(5) [see Fig. 2(b)].

Fast Coherent Inter-Site Transfer of Atomic Qubits

To extend our fast, low-heating *in situ* transfer to inter-site operations between separate S-traps, an additional spatial transport step is required. We analyze the transport-time dependence using long-distance transport measurements to determine the optimal transport time. An atom is loaded into the M-trap, and the M-trap is then moved back and forth over 35 μm for a total 51 one-way transport segments. As shown in Fig. 3(a), the survival increases with transport

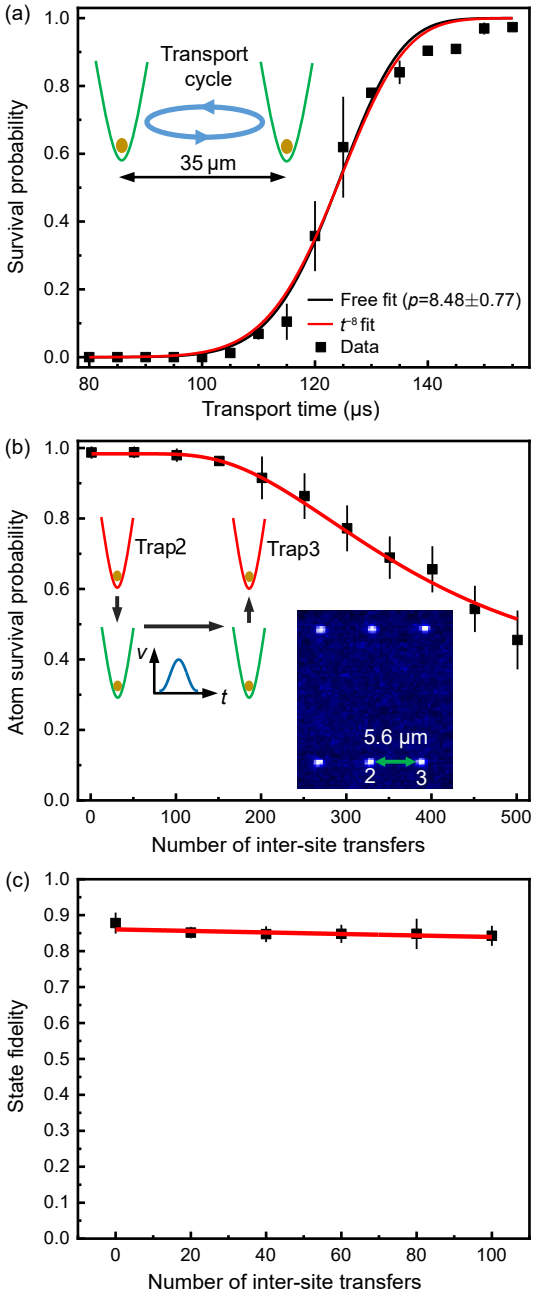

Fig. 3. Fast coherent inter-site transfer of a single atomic qubit (a) Measured survival probability with different transport times. The data are fitted using a heating scaling law $\Delta T_{\text{transport}} \propto t^{-p}$. The free fit yields $p = 8.48 \pm 0.79$ (black curve) is consistent with the theoretical t^{-8} prediction (red curve). Inset, schematic of long distance transport cycle. (b) Atom survival probability after different numbers of moves between the Trap2 and Trap3. Inset, the detailed qubit move procedure comprises two transfer processes and one transport process. (c) Internal-state fidelity after different numbers of moves fitted with exponential decay function.

time and saturates near 130 μs. For our STA trajectory [Eq. (1)], the transport-induced heating is expected to scale as t^{-8} derived in the Supplemental Material. To quantify the time dependence, we assume $\Delta T_{\text{transport}} = At^{-p}$ and substitute it into Eq. (3) to fit data, yielding an exponent of $p = 8.48 \pm 0.79$ in the free fit, consistent with the t^{-8} scaling in the Supplemental Material.

To verify the adaptability of the STA transfer waveform across different transport distances, we then demonstrate the full inter-site coherent transfer over a short distance within the array. We select two adjacent traps (Trap2 and Trap3) separated by 5.6 μm in the tweezer array (see Fig. 1), and repeatedly transfer the atom between them.

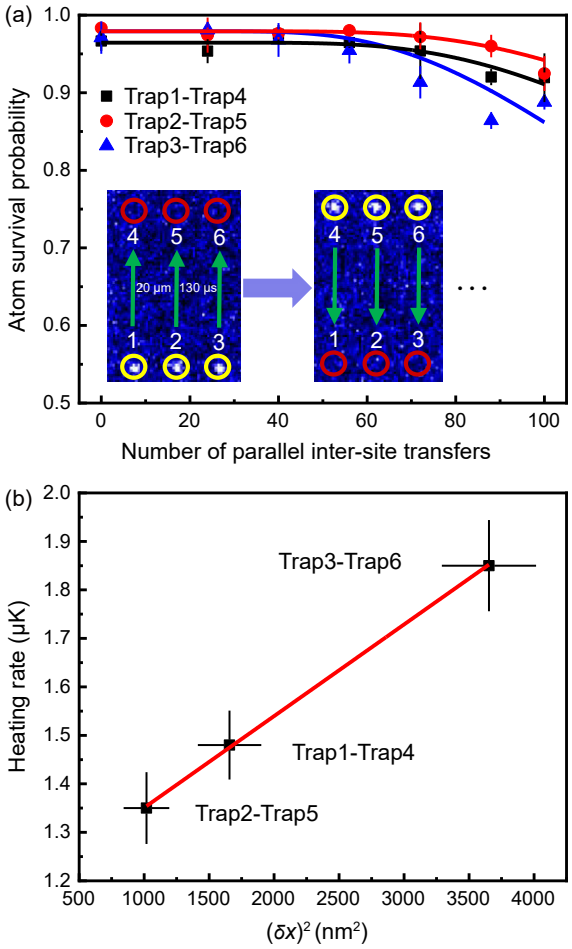

Fig. 4. Parallel inter-site transfer of atomic qubits (a) Atom survival probability after different numbers of parallel inter-site transfers. (b) Heating rates per inter-site transfer for the three groups as a function of the misalignment distance squared.

The moving trajectory of the M-trap follows Eq. (1) [see inset of Fig. 3(b)], with a transport time of 100 μs. The temperature of the atom gradually increases with the transfer count. After 500 inter-site transfers, the atom loss approaches 0.5. The single inter-site transfer heating rate is 0.783(17) μK, as determined by fitting the experimental data to Eq. (3), and induces a reduction of ~1% in the radial motional ground-state fraction after the first inter-site transfer. Since one complete inter-site transfer consists of two *in situ* transfer steps and one transport step, subtracting the measured *in situ* heating of both traps yields a single transport process heating rate of 0.627 μK, which induces a reduction of ~0.8% in the radial motional ground-state fraction after the first inter-site transfer. As before, we use quantum state tomography to characterize the inter-site transfer fidelity, the single-transfer fidelity is extracted to be 0.9998(1) [see Fig. 3(b)].

The ability to support parallel qubit transfer within the array is essential for quantum processors to enhance circuit efficiency. We use an AOD to generate three M-traps arranged horizontally with an equal spacing of 5.6 μm. These M-traps can simultaneously match Trap1–Trap3 or Trap4–Trap6 (shown in Fig. 1). Then, we transfer three qubits from the center to the edge of the fiber array. Due to the limited size of the fiber array, the moving distance is only 20 μm, and the total single inter-site transfer time is 150 μs. The heating rates per inter-site transfer for the three groups are 1.48(7) μK (Trap1–Trap4), 1.35(7) μK (Trap2– Trap5), and 1.89(9) μK (Trap3–Trap6), respectively [see Fig. 4(a)], which induce reductions of ~1.8%, ~1.7%, and ~2.3% in the radial motional ground-state fraction after the first inter-site transfer. We attribute this excess heating to a misalignment between the S-trap and M-trap, which arises from fabrication-induced

non-uniformity in the fiber array, leading to inconsistent trap spacing.

To understand and optimize the heating rate, we model the complete inter-site transfer as three sequential steps: *in situ* transfer, transport, and *in situ* transfer. The total heating is expressed as:

$$\begin{aligned}\Delta T &= \Delta T^{(1)}_{\text{transfer}} + \Delta T_{\text{transport}} + \Delta T^{(2)}_{\text{transfer}} \\ &= T^{(1)}_{\text{basic}} + \Delta T^{(1)}_{\text{mis}} + T_{\text{transport}}(D,t) + T^{(2)}_{\text{basic}} + \Delta T^{(2)}_{\text{mis}},\end{aligned}$$

where $\Delta T^{(1)}_{\text{basic}} = \Delta T^{(2)}_{\text{basic}}$ denotes the basic heating of a well-aligned *in situ* transfer step, $\Delta T^{(i)}_{\text{mis}}$ denote the misalignment-induced heating from the *in situ* transfers, and $\Delta T_{\text{transport}}$ corresponds to the heating generated during the M-trap motion.

For the well-aligned case, we take $\Delta T^{(1)}_{\text{basic}} + \Delta T^{(2)}_{\text{basic}} = 0.156(9)$ μK, which is the average of the two previously measured *in situ* heating rates. Under the harmonic approximation, a spatial misalignment between the S-trap and the M-trap introduces a position shift that yields:

$$\Delta T_{\text{mis}} = \Delta T^{(1)}_{\text{mis}} + \Delta T^{(2)}_{\text{mis}} = \frac{1}{2}\alpha m\omega_0^2\left[(\delta x_{\text{start}})^2 + (\delta x_{\text{target}})^2\right],$$

where α quantifies the non-adiabaticity of the transfer process and is a parameter dependent on the *in situ* transfer time. We performed a linear fit of the measured total heating against $(\delta x)^2$ [see Fig. 4(b)], obtaining $\Delta T^{\text{exp}}_{\text{transport}} \approx 1.01$ μK. On the other hand, based on our STA trajectory, the theoretical transport-induced heating follows the scaling $\Delta T_{\text{transport}} \propto D^2/(\omega_0^7 t^8)$. Using the transport heating $\Delta T_{\text{transport}} = 0.627$ μK extracted from the Trap2 and Trap3 experiments ($D = 5.6$ μm, $t = 100$ μs) as a reference, the scaling predicts $\Delta T^{\text{ideal}}_{\text{transport}} \approx 0.98$ μK for the parallel configuration ($D = 20$ μm, $t = 130$ μs), consistent with our experimental result, confirming that our model captures the dominant heating mechanisms. Compared to the constant-jerk trajectory with $\Delta T_{\text{transport}} \propto D^2/(\omega_0^3 t^4)$ and the adiabatic sinusoidal trajectory with $\Delta T_{\text{transport}} \propto D^2/(\omega_0^5 t^6)$ employed in several other experimentally realized schemes [9,20], our STA trajectory offers an improved scaling of $\Delta T_{\text{transport}} \propto D^2/(\omega_0^7 t^8)$, which facilitates a further reduction in the heating rate for a given transport distance and time.

Summary and Discussion

In summary, we experimentally demonstrate fast, coherent transfer of atomic qubits in a two-dimensional optical trap array, establishing a key capability for accelerating non-local qubit connectivity. Enabled by independent, site-resolved control of trap depths in a fiber array architecture [5], we realize *in situ* transfer between traps with a success probability exceeding 0.9999 in 10 μs, representing faster and higher-fidelity transfer compared to previous deep-trap-based adiabatic extraction from a shallow trap [3,7,19,20]. Furthermore, we have experimentally verified a transport trajectory that achieves a lower heating rate and a faster operation speed.

Currently, the heating of the *in situ* transfer is primarily caused by power fluctuations and interference between the S-trap and the M-trap, which can be improved through better power stabilization and larger detuning of the frequencies of the two beams. Moreover, the success probability of parallel inter-site transfer remains lower than single-atom inter-site transfer, primarily due to heating induced by the limited positioning accuracy of individual fibers. And the residual motional excitation after transport can further reduce the fidelity of the following Rydberg-mediated two-qubit gates. To solve this non-uniform trap spacing problem and scale up the atomic array, our next step is to employ femtosecond laser-written 3D photonic waveguides, which have the potential to support more than one thousand control channels [6,35]. This approach can reduce spatial non-uniformity to below 10 nm in our experimental setup, thereby enabling parallel inter-site transfer over hundreds of cycles. To further push the inter-site transfer capability to thousands of cycles, the inherent heating of the system can be systematically mitigated by enhanced sideband cooling and employing lower-noise, far-detuned traps, quantum optimal control [36–39] and machine-learning-based methods [20], ultimately pushing the transfer capability toward the fundamental limits set by background-gas collisions. Furthermore, residual heating is expected to be mitigated in deeper circuits by mid-circuit recooling [40] or atom replacement in a fault-tolerant architecture [1]. With these capabilities, together with fast, high-fidelity, individually addressed gates [5,41,42], our approach paves the way for a neutral-atom quantum computing architecture that simultaneously supports high quantum error correction cycle rates and efficient entanglement generation between logical qubits [7,43].

Acknowledgements

This work was supported by the National Key Research and Development Program of China (Grant No. 2021YFA1402001), the National Innovation Program for Quantum Science and Technology of China (Grant No. 2023ZD0300401), the National Natural Science Foundation of China (Grant Nos. 12004397, 12261131507, 12074391, U22A20257, 12121004, and 12241410), the CAS Project for Young Scientists in Basic Research (Grant No. YSBR-055), the Major Program (JD) of Hubei Province (Grant No. 2023BAA020), and the Strategic Priority Research Program of the Chinese Academy of Sciences (Grant No. XDB1690000).

References

[1] Bluvstein D, Geim A A, Li S H *et al*. 2026 *Nature* **649** 39
[2] Anand S, Bradley C E, White R *et al*. 2024 *Nat. Phys.* **20** 1744
[3] Reichardt B W, Paetznick A, Aasen D *et al*. 2025 arXiv: 2411.11822 [quant-ph]
[4] Wu X L, Liang X H, Tian Y Q, Yang F, Chen C, Liu Y C, Zheng M K, and You L 2021 *Chin. Phys. B* **30** 020305
[5] Li X, Hou J Y, Wang J C, Wang G W, He X D, Zhou F, Wang Y B, Liu M, Wang J, Xu P, and Zhan M S 2025 *Nat. Commun.* **16** 9728
[6] Ma D Q, Jie Q X, Hu Y D *et al*. 2025 *Sci. China-Phys. Mech. Astron.* **69** 220314
[7] Bluvstein D, Evered S J, Geim A A *et al*. 2024 *Nature* **626** 58
[8] Zhou H Y, Zhao C, Cain M *et al*. 2025 *Nature* **646** 303
[9] Bluvstein D, Levine H, Semeghini G *et al*. 2022 *Nature* **604** 451
[10] Baspin N and Krishna A 2022 *Phys. Rev. Lett.* **129** 050505
[11] Xu Q, Bonilla Ataides J P, Pattison C A *et al*. 2024 *Nat. Phys.* **20** 1084
[12] Baspin N and Krishna A 2022 *Quantum* **6** 711
[13] Saffman M 2025 arXiv: 2505.11218 [quant-ph]
[14] D'Angelis F M, Pinheiro F A, Guéry-Odelin D, Longhi S, and Impens F 2020 *Phys. Rev. Res.* **2** 033475
[15] Hwang H, Byun A, Park J, de Léséleuc S, and Ahn J 2023 *Optica* **10** 401
[16] Klostermann T, Cabrera C R, von Raven H, Wienand J F, Schweizer C, Bloch I, and Aidelsburger M 2022 *Phys. Rev. A* **105** 043319
[17] Lengwenus A, Kruse J, Schlosser M, Tichelmann S, and Birkl G 2010 *Phys. Rev. Lett.* **105** 170502
[18] Pagano A, Jaschke D, Weiss W, and Montangero S 2024 *Phys. Rev. Res.* **6** 033282
[19] Yang J H, He X D, Guo R J *et al*. 2016 *Phys. Rev. Lett.* **117** 123201
[20] Manetsch H J, Nomura G, Bataille E, Lv X, Leung K H, and Endres M 2025 *Nature* **647** 60
[21] Beugnon J, Tuchendler C, Marion H *et al*. 2007 *Nat. Phys.* **3** 696
[22] Ness G, Shkedrov C, Florshaim Y, and Sagi Y 2018 *New J. Phys.* **20** 095002
[23] Hwang S, Hwang H, Kim K *et al*. 2025 *Opt. Quantum* **3** 64
[24] Cicali C, Calzavara M, Cuestas E *et al*. 2025 *Phys. Rev. Appl.* **24** 024070
[25] Couvert A, Kawalec T, Reinaudi G, and Guéry-Odelin D 2008 *EPL* **83** 13001
[26] Tuchendler C, Lance A M, Browaeys A, Sortais Y R P, and Grangier P 2008 *Phys. Rev. A* **78** 033425
[27] Thew R T, Nemoto K, White A G, and Munro W J 2002 *Phys. Rev. A* **66** 012303
[28] Hofmann H F and Takeuchi S 2004 *Phys. Rev. A* **69** 042108
[29] Yu S, Xu P, Liu M, He X D, Wang J, and Zhan M S 2014 *Phys. Rev. A* **90** 062335
[30] Guo R J, He X D, Sheng C *et al*. 2020 *Phys. Rev. Lett.* **124** 153201

[31] Carruthers P and Nieto M M 1965 *Am. J. Phys.* **33** 537
[32] Endres M, Bernien H, Keesling A *et al*. 2016 *Science* **354** 1024
[33] Barredo D, Lienhard V, de Léséleuc S *et al*. 2018 *Nature* **561** 79
[34] Holman A, Xu Y, Sun X *et al*. 2026 *Nature* **649** 859
[35] Gattass R and Mazur E 2008 *Nat. Photon.* **2** 219
[36] Lam M R, Peter N, Groh T *et al*. 2021 *Phys. Rev. X* **11** 011035
[37] Torrontegui E, Ibáñez S, Chen X, Ruschhaupt A, Guéry-Odelin D, and Muga J G 2011 *Phys. Rev. A* **83** 013415
[38] Bowler R, Gaebler J, Lin Y, Tan T R, Hanneke D, Jost J D, Home J P, Leibfried D, and Wineland D J 2012 *Phys. Rev. Lett.* **109** 080502
[39] Walther A, Ziesel F, Ruster T, Dawkins S T, Ott K, Hettrich M, Singer K, Schmidt-Kaler F, and Poschinger U 2012 *Phys. Rev. Lett.* **109** 080501
[40] Lin R, Li Y, Zheng L T *et al*. 2026 arXiv: 2603.01612 [quant-ph]
[41] Radnaev A G, Chung W C, Cole D C *et al*. 2025 *PRX Quantum* **6** 030334
[42] Zhang B C, Peng P, Paul A, and Thompson J D 2024 *Optica* **11** 227
[43] Cain M, Xu Q, King R, Picard L R B, Levine H, Endres M, Preskill J, Huang H Y, and Bluvstein D 2025 arXiv: 2603.28627 [quant-ph]